Hindawi
Geofluids
Volume 2023, Article ID 7256937, 10 pages
https://doi.org/10.1155/2023/7256937

Research Article

The Seepage Evolution Mechanism of Variable Mass of Broken Rock in Karst Collapse Column under the Influence of Mining Stress

Li Xiao-Lei,[1] Li Xin-Lei,[1] Wang Yue,[2] Peng Wei-Hang,[3] Fan Xuan,[2,4] Cao Zheng-Zheng,[2,4] and Liu Rui-Fu[5]

[1]*Zhaogu No.2 Mine, Henan Energy Coking Coal Company, Jiaozuo, 454000 Henan, China*
[2]*Henan Key Laboratory of Underground Engineering and Disaster Prevention, Henan Polytechnic University, Jiaozuo 454000, China*
[3]*School of Physics & Electronic Information Engineering, Henan Polytechnic University, Jiaozuo 454000, China*
[4]*Collaborative Innovation Center of Coal Work Safety and Clean High Efficiency Utilization, Jiaozuo, 454000 Henan, China*
[5]*Structural and Fire Safety Engineering, The University of Edinburgh, UK*

Correspondence should be addressed to Cao Zheng-Zheng; hpu_zzc@126.com

Received 3 August 2022; Revised 21 December 2022; Accepted 23 March 2023; Published 12 April 2023

Academic Editor: Liang Xin

When the collapse column of overburden is disturbed by the working face, the grain loss in the karst collapse column occurs by the dissolution and corrosion of groundwater, thereby inducing the water inrush disaster. The test samples are prepared based on the fractal theory and the Talbol grading theory, and the seepage evolution law of fractured rock in collapse column under triaxial stress is studied, by employing the triaxial seepage test equipment. Besides, the seepage mechanics model of broken rock is established and calculated in the COMSOL Multiphysics, and the water-conducting channel under mass loss condition in the collapse column is further elucidated. The research results indicate that the loss ratio of mass is inversely proportional to the Talbol power index, and grain mass loss rate increases with the decrease of the Talbol power index. During the infiltration process, the evolution of pore structure is related with grain size distribution. With the increase of the Talbol power index, the overall porosity increases. Grain loss is an internal factor in seepage loss stability. Flow speed is accelerating, and seepage pathways are communicated with each other to induce the water inrush disaster.

1. Introduction

Collapse column is a special geological structure in the coal field of North China. Under the mining disturbance of the working face and overlying aquifer, collapse column tends to be activated, becoming a pathway between the overlying aquifer and stope, threatening the safety of coal mining [1]. With the extension in deep coal mines, water inrush disasters in the collapse column become more serious [2]. Water inrush reflects seepage stability and loss of water in a broken rock under the mining disturbance.

Many experts and scholars have done many research on this aspect. Yin et al. [3] established a thick-walled cylinder mechanical model of the collapse column and obtained a theoretical criterion of water inrush. Bai et al. [4] proposed a fluid structure "plug model," and the influence of multifield coupling should also be considered [5]. Zhu and Wei [6] and Yang et al. [7] studied the water inrush with the COMSOL Multiphysics and studied the formation process and evolution law of the water inrush channel of the working face. In terms of the research on permeability characteristics, Zhu et al. [8], Chen et al. [9], Ma et al. [10, 11], and Wu et al. [12] carried out a laboratory research on the permeability characteristics of broken rock and achieved variation rule of this aspect with time. Zhang et al. [13, 14] used the improved seepage test equipment to obtain grain change rule and distribution characteristics of filling material in the collapse column under the condition of graded loading and

Figure 1: Permeability test system for broken rock mass.

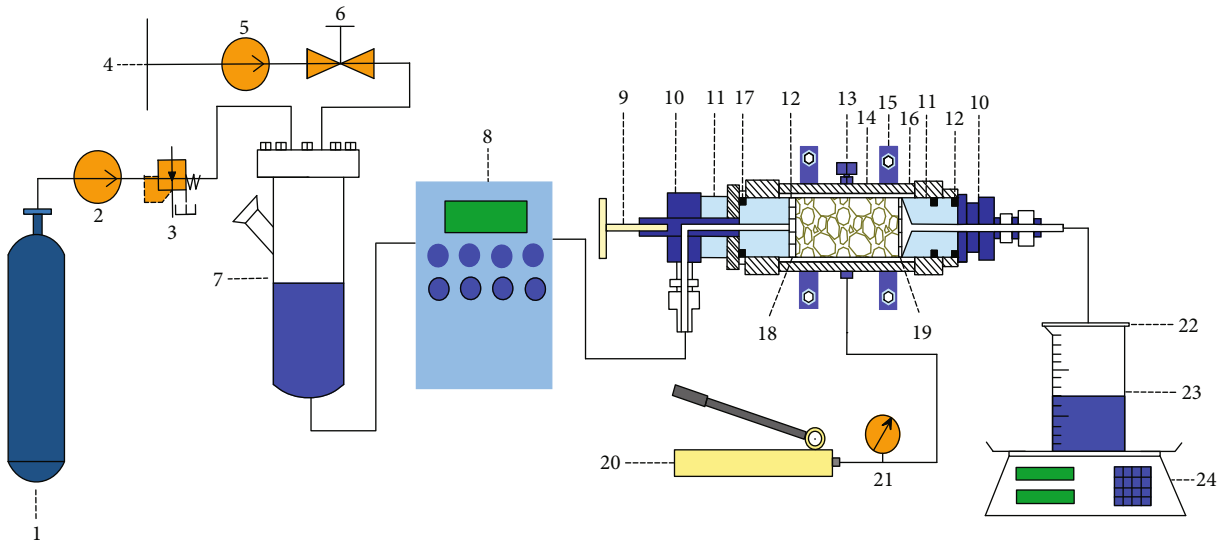

Figure 2: Schematic diagram of permeability test for broken rock mass.

different water pressure. Yu et al. [15] analyzed the influence of factors such as salt content, cement content, and rock grain size distribution on permeability characteristics. Feng et al. [16] analyzed the permeability characteristics and water intrusion and obtained the change law of mass loss with permeability. Zhang et al. [17] studied the relationship of pressure gradient with permeability in coal mining.

However, the change law of confining pressure with seepage characteristics under triaxial stress is seldom considered in previous permeability tests; besides, cementation in broken grains is not considered in most of them [18–21]. In practical engineering, collapse column is a cemented body formed by gradual compaction and filling cementation [22–24]. Therefore, this paper studies the seepage evolution law of the cemented broken rock mass under mining action, such as different confining pressures, degree of compaction and cementation, and grain size distribution of the broken rock mass.

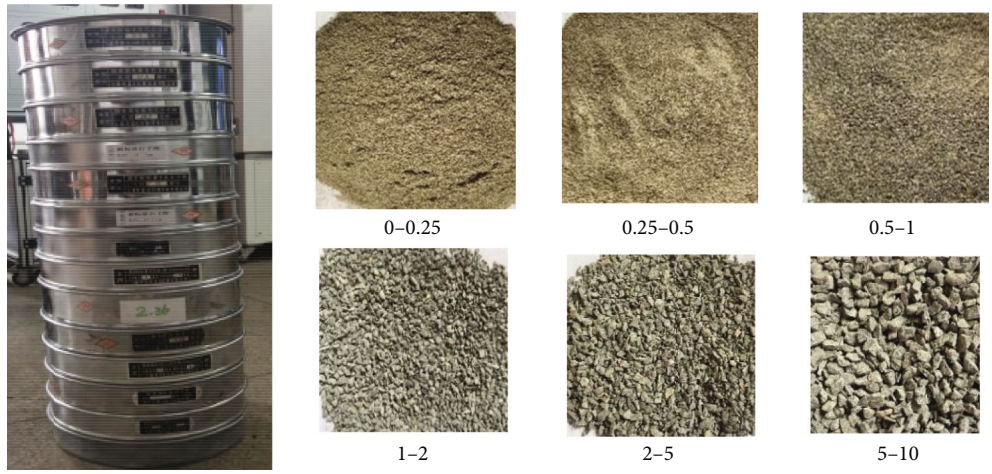

Figure 3: Screened samples with different grain sizes.

Table 1: Grain quality under different n.

n	Grain mass of each grain size range (g)					
	0-0.25 mm	0.25-0.5 mm	0.5-1 mm	1-2 mm	2-5 mm	5-10 mm
0.2	133.89	19.92	22.87	26.27	40.81	36.25
0.4	64.03	20.45	27.00	35.61	65.12	67.80
0.6	30.61	15.79	23.94	36.27	78.12	95.27
0.8	14.64	10.85	18.89	32.89	83.55	119.19

2. Laboratory Test

2.1. Test System. The self-developed seepage equipment system (Figures 1 and 2) is adopted, which contains five main parts, namely, confining pressure loading system, composed of the hydraulic manual pump and hydraulic flow meter, providing stable and adjustable confining pressure; osmotic pressure control system; the penetrator is the core device of this experiment; the data acquisition; and the filling grain collection system is mainly composed of the filter screen, oven, and electronic scale.

2.2. Sample Preparation. Before the test, standard screening machine is used to screen 6 kinds of broken rock grains with diameters according to actual conditions, and samples with different grain sizes are shown in Figure 3. According to the Talbol theoretical formula, the grain mass distribution of the rock grain size range of each size (Table 1) is obtained.

2.3. Law of Grain Mass Loss. Figure 4 reflects the evolution law of the mass rate of lost grains of each sample under the action of different coaxial displacements. This is mainly due to smaller n samples, and large grains in the sample quality percentage are small. The residual rock grains in the sample flowed out, and the change rate of mass lost decreases gradually.

As can be seen in Figure 5, the mass loss of small grain size accounts for a large proportion in the grain migration process, and the mass loss of grains gradually decreases with the increase in the Talbol index n. Grain size range of $0 \sim 0.25$ mm is the most obvious, and the mass of lost grains at all levels is 51.28, 38.71, 30.62, and 26.13 g, respectively.

2.4. Influence of Grain Loss on Porosity. Figure 6 shows the porosity time curve in the osmotic process. Pore rate decreases with increasing axial displacement (axial displacement is small) and a low degree of compaction. The porosity of the samples decreases with the augmentation of axial displacement. Under the action of higher confined pressure, the deformation of rock samples is greater, the water inrush channel is blocked, and the fine grains need to overcome greater resistance to overcome.

2.5. Influence of Different Cementation Strengths on Seepage Characteristics. Figure 7(a) shows the rate evolution of mass lost with various bonding strengths. The factor of the sample elevates greatly with the decrease of the bonding strength of the sample. The interaction between grains is small, and the pore structure of the sample has low stability.

Figure 7(b) shows the porosity evolution of samples with different cementation strengths. The stability of the pore structure of the sample with low cementation strength decreases, and the porosity increases significantly.

The permeability tests show that grain migration is the reason for mass seepage and loss and also a key factor for water inrush. As the main water channel after a seepage disaster, the whole water inrush process contains initial seepage, seepage surge, and seepage stability, shown in Figure 8.

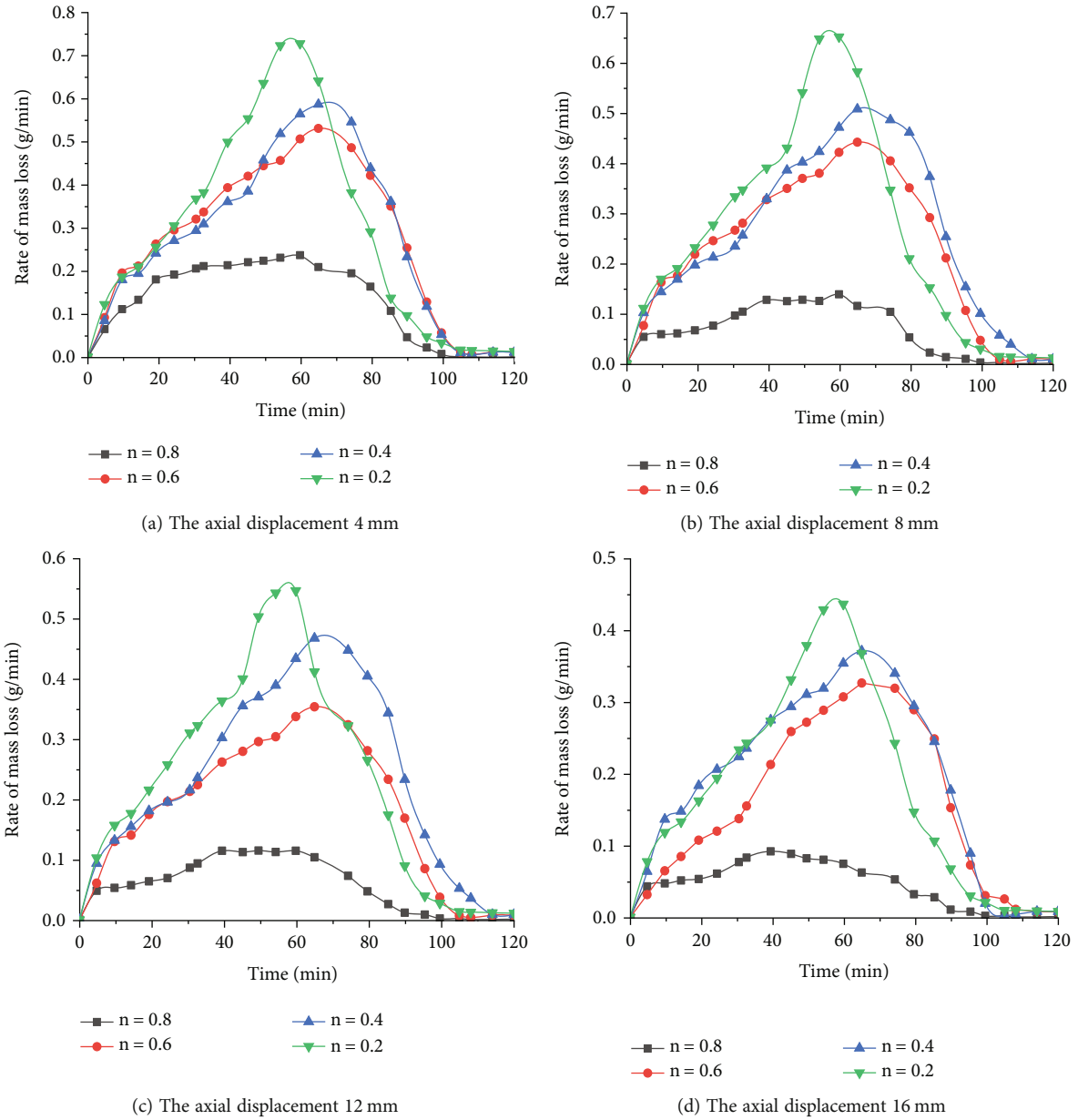

(a) The axial displacement 4 mm

(b) The axial displacement 8 mm

(c) The axial displacement 12 mm

(d) The axial displacement 16 mm

Figure 4: Evolution curve of mass rate of lost grains under different axial displacements.

3. Variable Mass Mechanics Model for Collapse Column

3.1. Establishment of Mechanical Model

3.1.1. Fluid Equation of Motion. The equation of motion of a fluid is

$$q_f = -\frac{k}{\eta}\left(\nabla p + \rho_f g \nabla z\right). \tag{1}$$

In the formula, q_f represents the Darcy velocity of the fluid; η represents the dynamic viscosity of the fluid; p represents the pore pressure; k represents the permeability; ∇z represents the direction of the gravity unit vector.

3.1.2. Conservation Equation of Mass. The mass conservation of grains is

$$\left(\frac{3}{a}\frac{\partial(\mathrm{bc})}{\partial t} + \frac{\partial(c\phi)}{\partial t}\right) + \nabla \cdot \left(\mathrm{cq}_f\right) = \left(\frac{3}{a}\frac{\partial b}{\partial t} + \frac{\partial \phi}{\partial t}\right). \tag{2}$$

In the formula, b represents the crack width, ϕ represents the porosity of the matrix block, c represents the volume concentration of suspended grains, and a represents the side length of the matrix block.

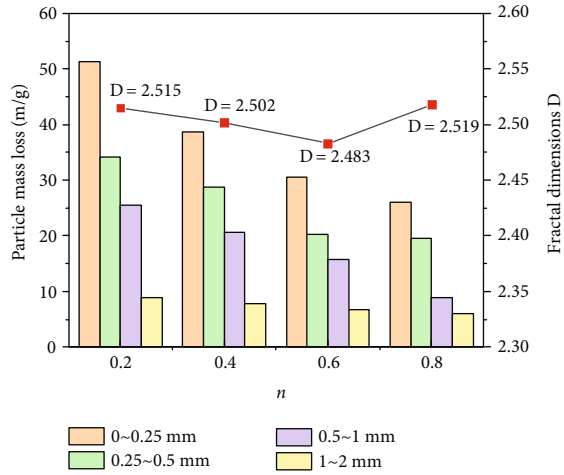

Figure 5: Fractal characteristics of grain loss.

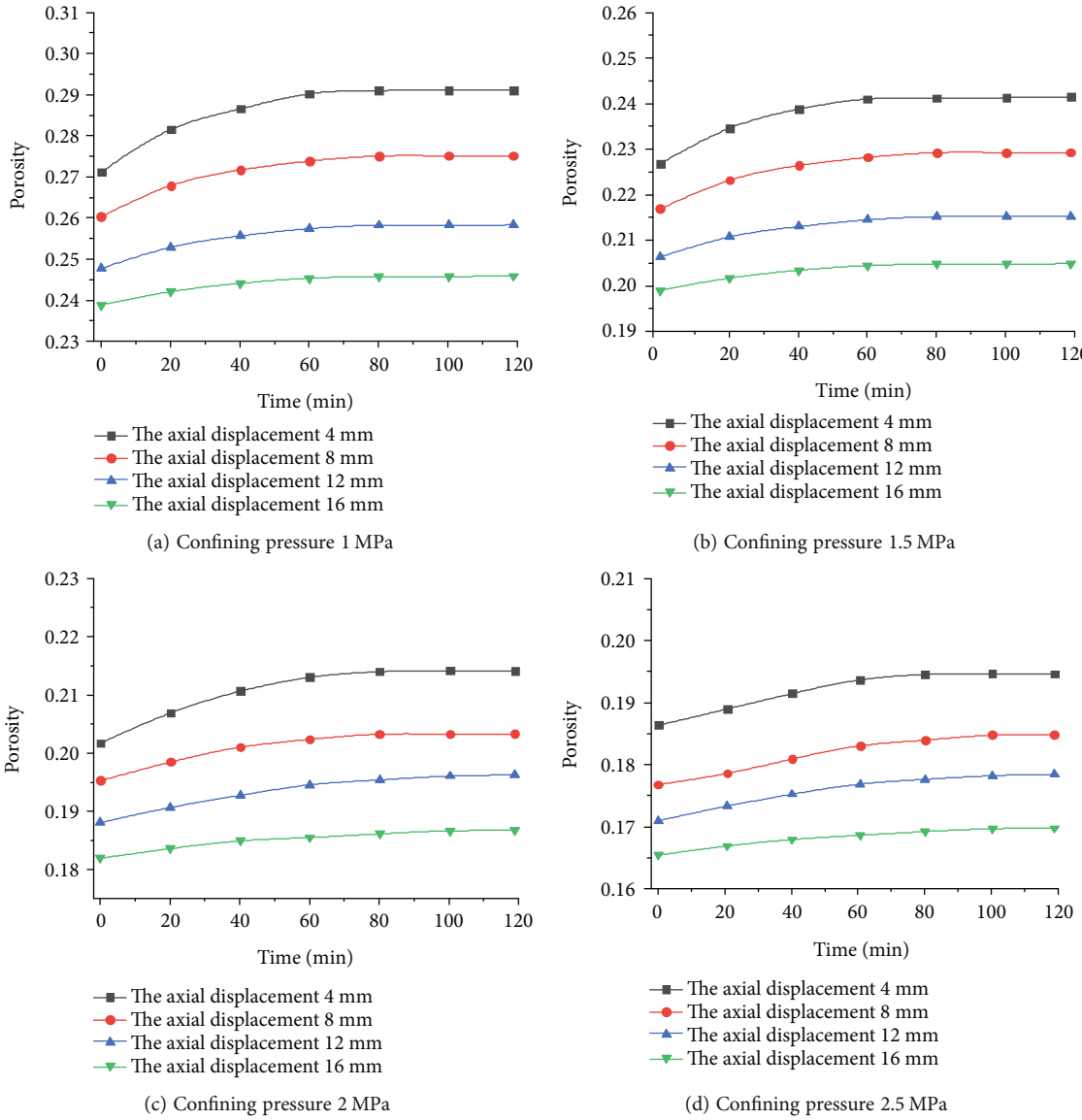

Figure 6: Porosity—time curve under different confining pressures.

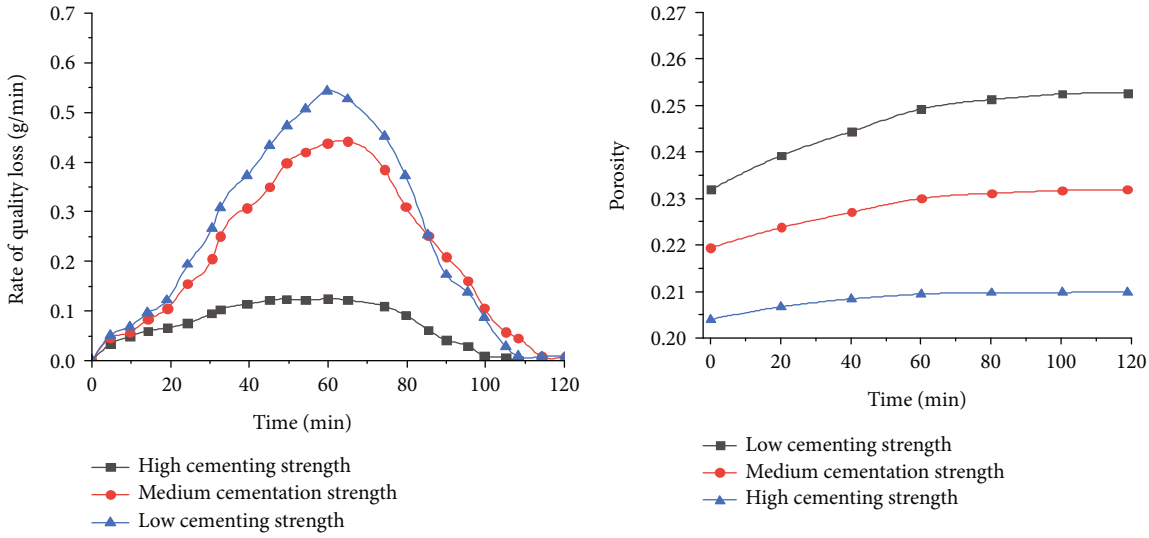

(a) Rate of mass loss (b) Porosity

Figure 7: Seepage evolution in various cemented strengths.

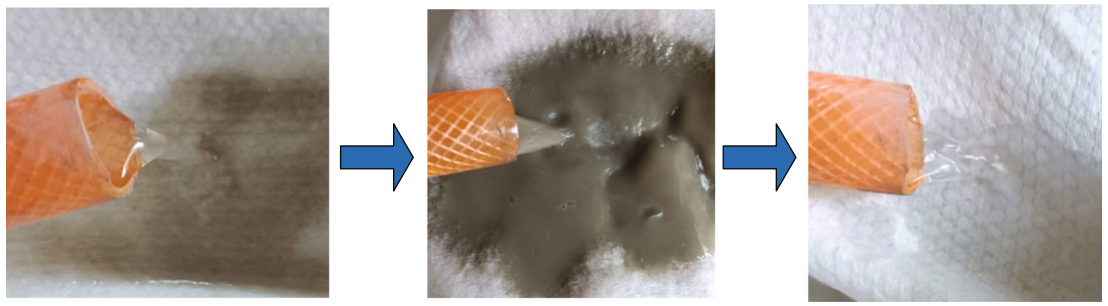

Figure 8: Evolution process in water inrush.

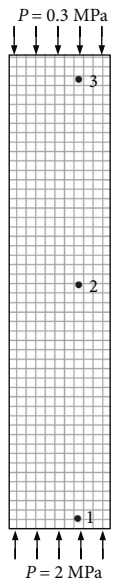

Figure 9: Numerical computation model.

Table 2: The value of the main parameters of the model.

Parameter	Collapse column	Unit
ρ	2260	g/m^3
E	1.0	GPa
μ	0.3	—
Matrix block length a	0.02	m
Pore corrosion coefficient λ_1	0.01	m^{-1}
Pore corrosion coefficient λ_2	0.01	m^{-1}
c	0.01	—
Initial permeability k_0	5×10^{-13}	m^2

3.1.3. Conservation in Fluid Mass.

$$\left(\frac{3}{a}\frac{\partial(b(1-c))}{\partial t} + \frac{\partial((1-c)\phi)}{\partial t}\right) + \nabla \cdot \left((1-c)q_f\right) = 0. \quad (3)$$

3.1.4. Porosity Evolution Equation

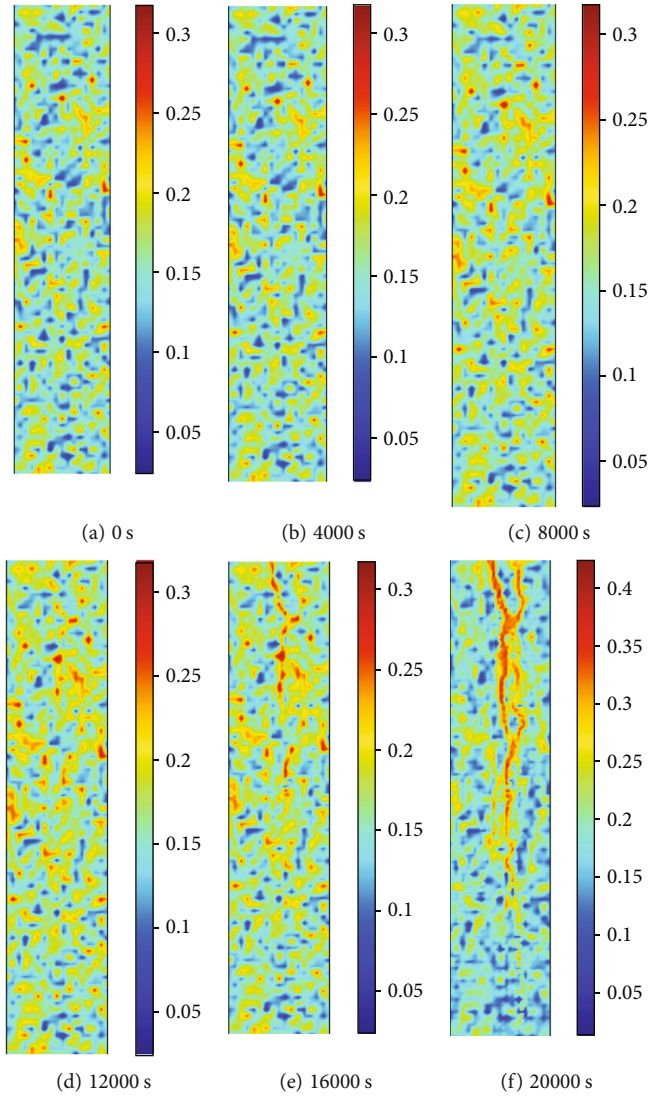

Figure 10: Porosity cloud map distribution.

(i) Vardoulakis et al. summarized the previous research results on the dissolution of porous media and gave the governing equation of pore evolution under the corrosion of porous media under grain migration

$$\frac{\partial \phi}{\partial t} = \lambda_1 \rho_s (\phi_{\max} - \phi) c|q|. \tag{4}$$

In the formula, λ_1 is a constant, and $|q|$ represents the seepage velocity absolute value.

3.1.5. Numerical Computation Model. Figure 9 is the computational model. The model diameter is 8 m, the height is 40 m, and the bottom water pressure is 2 MPa; the seepage boundary conditions are set, namely, the lower boundary water pressure $p = 2$ MPa; the top boundary is the water outlet; the pressure is set to air pressure, $p = 0.1$ MPa; and the left and right boundaries are impermeable boundaries. Six time points of 0 s, 4000 s, 8000 s, 12000 s, 16000 s, and 20000 s are selected as monitoring time points for calculation, and a position is selected at the bottom, middle, and top as monitoring points, respectively—point 2 (4.5, 20) and domain point 3 (4.5, 34.5). For the migration of grains in the model, the corresponding boundary conditions are set, namely, the lower boundary is the Dirichlet boundary and the upper boundary is the Newman boundary. The initial conditions are the pore water pressure at the lower boundary is 2 MPa, the upper boundary is the air pressure 0.1 MPa, the initial volume fraction of grains filled in the model pores is $c = 0.01$, and the matrix porosity satisfies the Weber distribution $m = 3$. The main parameters are in Table 2.

3.2. Numerical Simulation Results

3.2.1. Change Law of Porosity. Figure 10 is a cloud map of porosity distribution at different times. It is obvious that the pore structure is relatively stable before 12000 s. With the elevation of seepage time, broken rock grains migrate

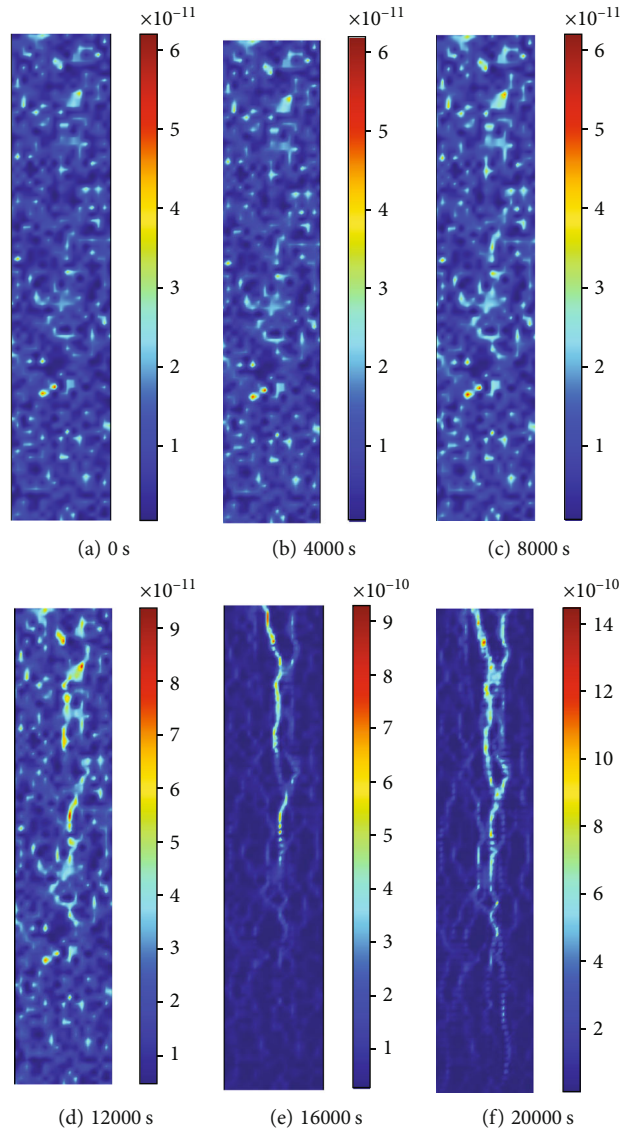

Figure 11: Permeability cloud map distribution.

gradually, and internal pore and skeleton structure are gradually damaged. Besides, the fine grains migrate, and seepage characteristics in broken rock are improved, thereby forming a potential water-conducting channel. According to the porosity change equation, mass migration is the main factor causing the porosity change, and the faster the mass migration, the faster the porosity change.

3.2.2. Change Law of Permeability. Figure 11 is a cloud map of permeability change with time. It is obvious that the permeability increases slowly firstly. Before $t = 12000$ s, maximum permeability is only 7.21×10^{-11} m^2. After $t = 12000$ s, the permeability increases quickly, and the maximum permeability of the model is 1.45×10^{-9} m^2, and the increasing range is 20.1 times. The broken rock inside the collapse column is lost, and several discontinuous seepage channels are formed.

4. Conclusions

(1) The test samples based on the fractal theory and the Talbol gradation theory are prepared, and the self-developed broken rock seepage equipment is employed to analyze the seepage evolution law of broken rock mass in the collapse column under triaxial stress. The grain mass loss rate is inversely proportional to n and axial displacement, and the grain mass loss rate increases as the value of n decreases

(2) As n value increases, porosity increases as a whole. Grain loss becomes the internal factor for the stability of seepage in the collapse column. Under the influence of water corrosion, grains inside the collapse column are continuously migrated and lost, forming several discontinuous seepage channels

(3) Based on the fluid mechanics and the COMSOL Multiphysics, the mechanics model of the collapse column is established, which clarifies the developing process of the water-conducting channel. Under the action of water corrosion, broken rock mass inside the collapse column is lost, and several discontinuous seepage channels are formed

Data Availability

The data used to support the findings of this study are included within the article.

Conflicts of Interest

The authors declare that they have no conflicts of interest.

Acknowledgments

This work was supported by the National Natural Science Foundation of China (52004082), the Program for the Scientific and Technological Innovation Team in Universities of Henan Province (23IRTSTHN005), the Project of Henan Key Laboratory of Underground Engineering and Disaster Prevention (Henan Polytechnic University), the Industry-University Cooperative Education Project of Ministry of Education (220901665160408), the Research and Practice Project of Educational and Teaching Reformation of Henan Polytechnic University in 2022 (Normal Finance-44).

References

[1] H. B. Bai, *Seepage Characteristics of Top Stratum of Ordovician System and Its Application Study as Key Aquifuge*, China University of Mining and Technology, Xuzhou, China, 2008.

[2] Y. Jiao and H. B. Bai, "Mechanism of delayed groundwater inrush from covered karst cave in coal seam floor," *Journal of China Coal Society*, vol. 38, no. S2, pp. 377–382, 2013.

[3] S. X. Yin, S. X. Wang, and Q. Wu, "Water inrush patterns and theoretic criteria of karstic collapse columns," *Chinese Journal of Rock Mechanics and Engineering*, vol. 23, no. 6, pp. 964–968, 2004.

[4] H. Bai, D. Ma, and Z. Chen, "Mechanical behavior of groundwater seepage in karst collapse pillars," *Engineering Geology*, vol. 164, pp. 101–106, 2013.

[5] B. H. Yao, L. C. Wang, J. P. Wei, Z. H. Li, and X. J. Liu, "A deformation-seepage-erosion coupling model for water outburst of karst collapse pillar and its application," *Journal of China Coal Society*, vol. 43, no. 7, pp. 2007–2013, 2018.

[6] W. C. Zhu and C. H. Wei, "Numerical simulation on mining-induced water inrushes related to geologic structures using a damage-based hydromechanical model," *Environmental Earth Sciences*, vol. 62, no. 1, pp. 43–54, 2011.

[7] T. H. Yang, S. K. Chen, W. H. Zhu, Z. H. Meng, and Y. F. Gao, "Water inrush mechanism in mines and nonlinear flow model for broken rocks," *Chinese Journal of Rock Mechanics and Engineering*, vol. 27, no. 7, pp. 1411–1416, 2008.

[8] W. H. Zhu, C. H. Wei, F. Z. Zhang, and T. H. Yang, "Invertigation of water inrush form karst subsidence column by using a coupled hydromechanical model," *Chinese Journal of Underground Space and Engineering*, vol. 5, no. 5, pp. 928–933, 2009.

[9] Z. Q. Chen, L. Z. Wang, H. L. Kong, and B. H. Yao, "Study on nonlinear seepage test of variable mass of broken rock," *Safety in Coal Mines*, vol. 45, no. 2, pp. 15–17, 2014.

[10] D. Ma, J. Wang, and Z. Li, "Effect of particle erosion on mining-induced water inrush hazard of karst collapse pillar," *Environmental Science and Pollution Research*, vol. 26, no. 19, pp. 19719–19728, 2019.

[11] D. Ma, H. Y. Duan, J. X. Zhang, X. J. Feng, and Y. L. Huang, "Experimental investigation of creep-erosion coupling mechanical properties of water inrush hazards in fault fracture rock masses," *Chinese Journal of Rock Mechanics and Engineering*, vol. 40, no. 9, pp. 1751–1763, 2021.

[12] J. Y. Wu, M. M. Feng, Z. H. Chen, B. Y. Yu, and G. S. Han, "Dissolution effects on the seepage property of broken mudstone," *Journal of Harbin Institute of Technology*, vol. 51, no. 2, pp. 117–125, 2019.

[13] T. J. Zhang, H. B. Shang, S. H. Li, J. H. Ren, R. Y. Bao, and L. Zhang, "Permeability characteristics of broken sandstone and its stability analysis under step loading," *Journal of China Coal Society*, vol. 41, no. 5, pp. 1129–1136, 2016.

[14] T. J. Zhang, X. F. Zhang, M. K. Pang, N. Liu, S. Zhang, and H. B. Gao, "Effect of particle loss on the pore structure and emergent behavior of karst column fills," *Journal of China Coal Society*, vol. 46, no. 10, pp. 3245–3254, 2021.

[15] B. Y. Yu, Z. H. Chen, J. Y. Wu, and L. Z. Wang, "Experimental study of non-Darcy flow seepage properties of cemented broken rocks with mass loss," *Journal of China University of Mining & Technology*, vol. 46, no. 2, pp. 321–327, 2017.

[16] M. M. Feng, J. Y. Wu, D. Ma, X. Ni, B. Yu, and Z. Chen, "Experimental investigation on the seepage property of saturated broken red sandstone of continuous gradation," *Bulletin of Engineering Geology and the Environment*, vol. 77, no. 3, pp. 1167–1178, 2018.

[17] B. Y. Zhang, H. B. Bai, and K. Zhang, "Study on the mechanism of delayed water inrush of collapse column under the influence of mining," *Journal of China University of Mining & Technology*, vol. 45, no. 3, pp. 447–454, 2016.

[18] M. M. Feng, J. Y. Wu, Z. Q. Chen, X. B. Mao, and B. Y. Yu, "Experimental study on the compaction of saturated broken rock of continuous gradation," *Journal of China Coal Society*, vol. 41, no. 9, pp. 2195–2202, 2016.

[19] Z. Cao, Y. Wang, H. Lin, Q. Sun, X. Wu, and X. Yang, "Hydraulic fracturing mechanism of rock mass under stress-damage-seepage coupling effect," *Geofluids*, vol. 2022, Article ID 5241708, 11 pages, 2022.

[20] Y. Xue, P. G. Ranjith, F. Gao, Z. Zhang, and S. Wang, "Experimental investigations on effects of gas pressure on mechanical behaviors and failure characteristic of coals," *Journal of Rock Mechanics and Geotechnical Engineering*, vol. 15, no. 2, pp. 412–428, 2023.

[21] A. Gang-jian, C. Zheng-zheng, D. Hong-fei, L. Guo-sheng, and L. Ao, "Mechanical response of surrounding rock of karst tunnel under stress-damage- seepage coupling effect," *Geofluids*, vol. 2022, Article ID 6879808, 11 pages, 2022.

[22] Y. Xue, S. Liu, J. Chai et al., "Effect of water-cooling shock on fracture initiation and morphology of high-temperature granite: application of hydraulic fracturing to enhanced geothermal systems," *Applied Energy*, vol. 337, article 120858, 2023.

[23] J. Liu, Y. Xue, Y. Fu, K. Yao, and J. Liu, "Numerical investigation on microwave-thermal recovery of shale gas based on a fully coupled electromagnetic, heat transfer, and multiphase flow model," *Energy*, vol. 263, article 126090, 2023.

[24] Y. Xue, J. Liu, X. Liang et al., "Influence mechanism of brine-gas two-phase flow on sealing property of anisotropic caprock for hydrogen and carbon energy underground storage," *International Journal of Hydrogen Energy*, vol. 48, no. 30, pp. 11287–11302, 2023.